Calculation of Wannier functions for fcc transition metals by Fourier transformation of Bloch functions

B. Sporkmann and H. Bross
Sektion Physik der Ludwig-Maximilians-Universität, Theresienstraße 37, D-80333 München, Germany
(Received 26 August 1993; revised manuscript received 6 December 1993)

A method is described for the calculation of generalized symmetry-adapted Wannier functions by Fourier transformation of Bloch functions obtained by standard first-principles techniques. An additional unitary transformation derived from a Slater-Koster-model Hamiltonian is introduced in order to deal with the nonanalytical behavior of the Bloch functions. The parameters of the Hamiltonian, which are the energy matrix elements of the Wannier functions, reproduce the first-principles band structure with high accuracy. It is considered in detail how problems caused by degeneracies have to be treated by an analysis of transformation properties at symmetry points. An application to fcc transition metals yields highly localized functions of d symmetry, an s function whose localization depends on the strength of relativistic effects, and less localized p functions.

INTRODUCTION

Since their introduction in 1937,[1] Wannier functions have been used in many theoretical models, e.g., in the theory of localized perturbations. However, there exist only few numerical realizations, most of them consisting of a direct calculation rather than a Fourier transformation of Bloch functions. The direct variational approach proposed by Kohn[2] has recently been applied by Modrak and Wojnecki to the d bands[3] and the d-s-band complex of copper and nickel.[4] These calculations yield convincing results for the d functions but a very extended s function possibly due to the neglect of p functions or to certain assumptions about the functional form of the Wannier functions outside the central muffin-tin sphere.

On the other hand, there have been only a few attempts to calculate Wannier functions for real crystals applying the Fourier transformation of Bloch functions, although this indirect approach could take advantage of the highly developed techniques of modern first-principles methods. Problems connected with the direct calculation like orthogonality and three-center corrections are automatically included.

However, problems arise from the fact that the Bloch functions labeled according to increasing energy are not analytic functions of the wave vector $\mathbf{k}$ at points of degeneracy. In order to avoid this difficulty Callaway and Hughes[5] developed a symmetry labeling scheme in their calculations for silicon, which required the interchange of band numbers even at points of quasidegeneracies thus leading to new discontinuities. Goodings and Harris[6] pointed out that this would be a complicated procedure in the case of transition metals and kept the usual scheme in their calculation for copper. Their results showed poorly localized Wannier functions certainly due to the nonanalytical behavior of the Bloch functions.

It has been proposed[7,8] that this item should be treated considering groups of bands rather than single bands. One of us has suggested earlier[9] that this should be done by employing the eigenvectors of a Slater-Koster-model Hamiltonian leading to Wannier functions of defined symmetry. In this work we give a detailed instruction how this can be carried out in a numerically successful way.

I. DEFINITION OF GENERALIZED WANNIER FUNCTIONS

At this stage we briefly want to summarize the concepts given in Ref. 9. The one-particle energies and wave functions may be known from a first-principles calculation by means of the approximate solution of an effective one-particle Schrödinger equation

$$\mathbf{H}\psi_{n\mathbf{k}} = E_{n\mathbf{k}}\psi_{n\mathbf{k}} \quad . \tag{1.1}$$

$\mathbf{H}$ is the effective one-particle-Hamiltonian, $E_{n\mathbf{k}}$ is the one-particle energy eigenvalue for wave vector $\mathbf{k}$ and band n, and $\psi_{n\mathbf{k}}$ denotes the corresponding one-particle wave function, which is also called a Bloch function.

As we are interested in a small number of bands we put these together into a band complex and look for a model Hamiltonian with the same eigenvalues $E_{n\mathbf{k}}$,

$$\sum_{\mu} H_{\nu\mu}(\mathbf{k})\; e(n,\mathbf{k})_{\mu} = E_{n\mathbf{k}}\; e(n,\mathbf{k})_{\nu} \quad , \tag{1.2}$$

where $e(n,\mathbf{k})_{\nu}$ are the eigenvectors. In the case of metals the definition of such a band complex imposes the introduction of an artificial cut in the band structure, which is in some respect ambiguous. This is of course done in an energy region far enough from the region of interest, so that it can be expected that the reproduction of the band structure will be adequate there.

The energies of the band complex at $\mathbf{k} = 0$ may be labeled by the irreducible representations of the point group $\Gamma^{(1)},\ldots,\Gamma^{(p)}$. Then the following symmetry properties are required:

0163-1829/94/49(16)/10869(8)/$06.00 ©1994 The American Physical Society

$$H(\alpha\mathbf{k}) = \Gamma(\alpha)\ H(\mathbf{k})\ \Gamma(\alpha)^{-1} \tag{1.3}$$

with

$$\Gamma(\alpha) \equiv \begin{pmatrix} \Gamma^{(1)}(\alpha) & & 0 \\ & \ddots & \\ 0 & & \Gamma^{(p)}(\alpha) \end{pmatrix} \quad , \tag{1.4}$$

where α denotes an element of the point group. So the dimension of the model Hamiltonian and the transformation matrices is the sum of the dimensions of the irreducible representations contained in the band complex. The H matrix is expanded into a Fourier series in the lattice vectors $\mathbf{R}$:

$$H(\mathbf{k}) = \sum_{\mathbf{R}} \varepsilon(\mathbf{R})\ e^{-i\mathbf{k}\cdot\mathbf{R}} \tag{1.5}$$

with similar symmetry requirements for the coefficient matrices:

$$\varepsilon(\alpha\mathbf{R}) = \Gamma(\alpha)\ \varepsilon(\mathbf{R})\,\Gamma(\alpha)^{-1} \quad . \tag{1.6}$$

The independent parameters $\varepsilon_{\mu\nu}(\mathbf{R})$ have to be obtained by a nonlinear least-squares fit of the eigenvalues (1.2) to the band structure energies. The reader familiar with lattice dynamics will note the close similarity between the dynamical matrix and the model Hamiltonian $H(\mathbf{k})$ and the polarization vector and $e(n,\mathbf{k})$, respectively.

Like in Ref. 9, we now define generalized symmetry-adapted Wannier functions using the eigenvectors of the model Hamiltonian and summing over the band complex:

$$a_\nu(\mathbf{r}-\mathbf{R}) = \frac{\Omega^{\frac{1}{2}}}{(2\pi)^{\frac{3}{2}}} \int_{BZ} d\mathbf{k}\, e^{-i\mathbf{k}\cdot\mathbf{R}} \sum_n e(n,\mathbf{k})^*_\nu\, \psi_{n\mathbf{k}}(\mathbf{r}) \quad , \tag{1.7}$$

where Ω denotes the volume of the Wigner-Seitz cell. As has been shown in Ref. 9, the Fourier coefficients in (1.5) are the energy matrix elements of the Wannier functions

$$\varepsilon_{\mu\nu}(\mathbf{R}) = \int a_\mu(\mathbf{r}-\mathbf{R})^*\ \mathbf{H}\ a_\nu(\mathbf{r})\ d^3r \quad . \tag{1.8}$$

In the following these will be called Slater-Koster parameters. The Wannier functions transform like basis functions of irreducible representations of the point group

$$\sum_\mu \Gamma(\alpha)_{\nu\mu}\, a_\mu(\mathbf{r}) = a_\nu(\alpha\mathbf{r}) \tag{1.9}$$

and obey the orthogonality relations:

$$\int a_\mu(\mathbf{r}-\mathbf{R}_i)^*\, a_\nu(\mathbf{r}-\mathbf{R}_j)\, d\mathbf{r} = \delta_{\nu\mu}\delta_{ij} \quad . \tag{1.10}$$

It is important to note that the model Hamiltonian and the Wannier functions are uniquely defined only by the choice of the independent Slater-Koster parameters. While there may always be various sets of parameters which reproduce the first-principles eigenvalues satisfactorily well, one can expect to obtain well localized Wannier functions only if the Fourier expansion (1.5) converges fast.

II. CONSTRUCTION OF THE WANNIER FUNCTIONS

A. Treatment of degeneracies

In the case of a degeneracy at the point $\mathbf{k}$ there exists an arbitrariness in the first-principles eigenfunctions as well as in the eigenvectors of the model Hamiltonian belonging to the degenerated energy. This arbitrariness is connected to the fact that the representations under which either of them transform are determined only up to equivalence. The group of $\mathbf{k}$ is the set of point operations which leave $\mathbf{k}$ invariant up to a reciprocal lattice vector: $G(\mathbf{k}) = \{\beta \,|\, \beta\mathbf{k} = \mathbf{k}+\mathbf{K}\}$. The degenerated Bloch functions transform in the following way:

$$\psi_{n\mathbf{k}}(\beta^{-1}\mathbf{r}) = \sum_{n'} \widetilde{D}_{\mathbf{k}}(\beta)_{nn'}\, \psi_{n'\mathbf{k}}(\mathbf{r}) \quad \text{for } \beta \in G(\mathbf{k}) \quad , \tag{2.1}$$

where the sum is extended over the degenerated states. The matrices $\widetilde{D}_{\mathbf{k}}(\beta)$ form an irreducible representation of $G(\mathbf{k})$, the dimension of which is the degree d of the degeneracy. When the first-principles Bloch functions are normalized on the Wigner-Seitz cell Ω the matrix elements can be obtained in the following way:

$$\widetilde{D}_{\mathbf{k}}(\beta)_{nn'} = \int_\Omega \psi^*_{n\mathbf{k}}(\mathbf{r})\ \psi_{n'\mathbf{k}}(\beta\mathbf{r}) \quad . \tag{2.2}$$

For the eigenvectors of the model Hamiltonian we define

$$D_{\mathbf{k}}(\beta)_{nn'} \equiv \sum_{\mu\nu} \Gamma(\beta)^{-1}_{\nu\mu}\ e(n,\mathbf{k})^*_\mu\ e(n',\mathbf{k})_\nu \quad . \tag{2.3}$$

$D_{\mathbf{k}}$ is an equivalent unitary irreducible representation of $G(\mathbf{k})$. So there exists a unitary transformation U with

$$D_{\mathbf{k}}(\beta) = U\ \widetilde{D}_{\mathbf{k}}(\beta)\ U^{-1} \quad \text{for all } \beta \in G(\mathbf{k}) \quad . \tag{2.4}$$

It is shown in the Appendix that the symmetry of the Wannier-functions (1.9) requires

$$D_{\mathbf{k}}(\beta) = \widetilde{D}_{\mathbf{k}}(\beta) \quad . \tag{2.5}$$

This condition can be fulfilled if the inverse of the unitary transformation U is applied to the eigenvectors $e(n,\mathbf{k})_\nu$, thus defining a new set of degenerated eigenvectors $\widetilde{e}(n,\mathbf{k})_\nu$. These can be found using a projection operator technique:

$$\begin{aligned}
\frac{d}{g} \sum_{\beta\in G(\mathbf{k})} \widetilde{D}_{\mathbf{k}}(\beta)_{nn} \sum_\mu \Gamma(\beta)^{-1}_{\nu\mu}\, e(n,\mathbf{k})_\mu &= \frac{d}{g} \sum_{\beta\in G(\mathbf{k})} \widetilde{D}_{\mathbf{k}}(\beta)_{nn} \sum_{n'} D_{\mathbf{k}}(\beta)_{nn'}\, e(n',\mathbf{k})_\nu \\
&= \frac{d}{g} \sum_{\beta\in G(\mathbf{k})} \widetilde{D}_{\mathbf{k}}(\beta)_{nn} \sum_{n'pq} U_{np}\, \widetilde{D}_{\mathbf{k}}(\beta)_{pq}\, U^{-1}_{qn'}\, e(n',\mathbf{k})_\nu \\
&= \sum_{n'pq} \delta_{np}\,\delta_{nq}\, U_{np}\, U^{-1}_{qn'}\, e(n',\mathbf{k})_\nu = U_{nn} \sum_{n'} U^{-1}_{nn'}\ e(n',\mathbf{k})_\nu = U_{nn}\, \widetilde{e}(n,\mathbf{k})_\nu \quad .
\end{aligned} \tag{2.6}$$

g denotes the order of $G(\mathbf{k})$. The summations are extended over the degenerated band indices. In the third step we have used the orthogonality relations for irreducible representations of finite groups. Normalization yields the new eigenvectors $\widetilde{e}(n,\mathbf{k})_\nu$ up to a phase factor. The relative phase factors are determined comparing the off-diagonal elements calculated according to (2.3) with those from (2.2).

In this way the freedom is removed which lies in the arbitrary orientation of the degenerated eigenfunctions leading to the failure of the $\mathbf{k}\cdot\mathbf{p}$ procedure in the case of a degeneracy. Thus we assume to obtain smooth functions in $\mathbf{k}$ space and as a consequence well localized Wannier functions. This assumption will be confirmed by the numerical results.

B. The phase of the Bloch functions

After the nonanalyticity of the original Bloch functions has been treated by a suitable linear combination of those, we are still free to multiply them by an arbitrary phase factor as long as we do not introduce new discontinuities. As was suggested by Blount,[7] we want to fix this phase in a manner that leads to best localized Wannier functions in the sense that the mean square radius

$$r^2_{\nu\nu} = \int r^2\,|a_\nu(\mathbf{r})|^2 d\mathbf{r} \tag{2.7}$$

is minimized. We define quasi-Bloch functions in the following way:

$$\phi_{\nu\mathbf{k}}(\mathbf{r}) = \sum_n e(n,\mathbf{k})^*_\nu\,\psi_{n\mathbf{k}}(\mathbf{r}) \quad , \tag{2.8}$$

with a lattice-periodic part $u_{\nu\mathbf{k}}$:

$$\phi_{\nu\mathbf{k}}(\mathbf{r}) = e^{i\mathbf{k}\cdot\mathbf{r}}\,u_{\nu\mathbf{k}}(\mathbf{r}) \quad . \tag{2.9}$$

If no contributions from discontinuities occur, which we assume from the foregoing, the operation of a power of $\mathbf{r}$ on a Wannier function can be written[7]

$$r^n_j a_\nu(\mathbf{r}) = \frac{\Omega^{\frac{1}{2}}}{(2\pi)^{\frac{3}{2}}}\int_{BZ} d\mathbf{k} e^{i\mathbf{k}\cdot\mathbf{r}}\left(i\frac{\partial}{\partial k_j}\right)^n u_{\nu\mathbf{k}}(\mathbf{r}) \quad . \tag{2.10}$$

This leads to the following expression for the mean square radius:

$$r^2_{\nu\nu} = \frac{-\Omega}{(2\pi)^3}\int_{BZ} d\mathbf{k}\int_{BZ} d\mathbf{k}'\,\delta(\mathbf{k}-\mathbf{k}') \times\nabla_{\mathbf{k}}\,\nabla_{\mathbf{k}'}\int_\Omega d\mathbf{r}\,u^*_{\nu\mathbf{k}'}(\mathbf{r})\,u_{\nu\mathbf{k}}(\mathbf{r}) \quad . \tag{2.11}$$

In general the minimization of this expression would have to be carried out numerically by introducing phase factors in Eq. (2.8). However, for the case of inversion symmetry Teichler[10] has given an argument which shows how the phase is to be chosen. We expand the $u_{\nu\mathbf{k}}$ into plane waves:

$$u_{\nu\mathbf{k}}(\mathbf{r}) = \sum_j V(\nu,\mathbf{k})_j\,e^{i\mathbf{K}_j\cdot\mathbf{r}} \quad . \tag{2.12}$$

In a crystal with inversion center the coefficients $V(\nu,\mathbf{k})_j$ can be chosen real. So we can write

$$V(\nu,\mathbf{k})_j = e^{i\chi_\nu(\mathbf{k})}\,\widetilde{V}(\nu,\mathbf{k})_j \quad , \tag{2.13}$$

where $\widetilde{V}(\nu,\mathbf{k})_j$ is real. So we get for the mean square radius

$$\begin{aligned} r^2_{\nu\nu} &= \frac{-\Omega}{(2\pi)^3}\int d\mathbf{k}\int d\mathbf{k}'\delta(\mathbf{k}-\mathbf{k}')\nabla_{\mathbf{k}}\,\nabla_{\mathbf{k}'}\sum_{jj'} V(\nu,\mathbf{k})_j\,V(\nu,\mathbf{k}')^*_{j'}\int_\Omega e^{i(\mathbf{K}_j-\mathbf{K}_{j'})\cdot\mathbf{r}}d\mathbf{r} \\ &= \int d\mathbf{k}\sum_j |\nabla_{\mathbf{k}}\,\widetilde{V}(\nu,\mathbf{k})_j|^2 + \int d\mathbf{k}\,|\nabla_{\mathbf{k}}\,\chi_\nu(\mathbf{k})|^2 \quad . \end{aligned} \tag{2.14}$$

It follows that $r^2_{\nu\nu}$ takes on its minimum value when the expansion coefficients in (2.12) are chosen real. This is equivalent to the choice of real Wannier functions in the case of even representations and purely imaginary ones for odd representations.

C. Numerical representation

In the MAPW procedure,[11,12] which we used as the first-principles method to determine the band structure and the Bloch functions, the following Ritz ansatz is made for the Bloch function in the central cell:

$$\begin{aligned} \psi_{n\mathbf{k}}(\mathbf{r}) = &\sum_j v(n,\mathbf{k})_j\left\{e^{i(\mathbf{k}+\mathbf{K}_j)\mathbf{r}} - \Theta(r_0-r)\sum_{L=0}^{L_{\max}} i^l\,c_L\,j_l(|\mathbf{k}+\mathbf{K}_j|r)\,Y_L(\mathbf{k}+\mathbf{K}_j)\,Y_L(\mathbf{r})\right\} \\ &+\Theta(r_0-r)\sum_{L=0}^{L_{\max}} i^l\,c_L\sum_E A_{EL}(n,\mathbf{k})R_{El}(r)\,Y_L(\mathbf{r}) \quad . \end{aligned} \tag{2.15}$$

r_0 is the muffin-tin radius, R_{EL} are solutions of the radial Schrödinger equation for certain energies E, j_l are the spherical Bessel functions, and Y_L are real spherical harmonics with normalization factors c_L. The most important features of the wave functions obtained from this procedure are that they are orthogonal to the core states and everywhere differentiable in $\mathbf{r}$, so the Wannier functions will have the same properties. The plane wave coefficients $v(n,\mathbf{k})_j$ and the radial coefficients $A_{EL}(n,\mathbf{k})$ as well as the eigenvectors of the model Hamiltonian are real so there remains only a trivial choice between $+1$ and -1 for the phase. This is of course determined in a way to produce a smooth function in $\mathbf{k}$ space. We choose a certain small $\mathbf{r}$ for which we demand that $\sum_n e_\nu(n,\mathbf{k})^* \psi_{n\mathbf{k}}(\mathbf{r})$ do not change sign for all $\mathbf{k}$ in the irreducible wedge.

The special form of the Bloch functions described above implies that the Wannier functions are composed of two parts. One part confined to the muffin-tin spheres consists of radial functions and spherical harmonics up to a limiting value of angular momentum. After replacing the $\mathbf{k}$ integration by a sum the other one remains a superposition of a large (700) number of symmetrized plane waves covering the whole space,

$$a_\nu(\mathbf{r}) = \sum_{\mathbf{R}} \sum_L f_{\nu L\mathbf{R}}(|\mathbf{r}-\mathbf{R}|)\, Y_L(\mathbf{r}-\mathbf{R}) + \sum_{\mathbf{k}} \sum_j v_{\nu\mathbf{k}+\mathbf{K}_j}\, e^{i(\mathbf{k}+\mathbf{K}_j)\cdot\mathbf{r}} \tag{2.16a}$$

with

$$v_{\nu\mathbf{k}+\mathbf{K}_j} = \sum_n e(n,\mathbf{k})_\nu\, v(n,\mathbf{k})_j \tag{2.16b}$$

and

$$f_{\nu L\mathbf{R}}(r) = \Theta(r_0 - r)\, i^l\, c_L \left\{ \sum_E \left(\sum_{\mathbf{k}} e^{-i\mathbf{k}\cdot\mathbf{R}} \sum_n e(n,\mathbf{k})_\nu\, A_{EL}(n,\mathbf{k}) \right) R_{El}(r) - \sum_{\mathbf{k}} e^{-i\mathbf{k}\cdot\mathbf{R}} \sum_j v_{\nu\mathbf{k}+\mathbf{K}_j} j_l(|\mathbf{k}+\mathbf{K}_j|r) Y_L(\mathbf{k}+\mathbf{K}_j) \right\}. \tag{2.16c}$$

In the central muffin-tin sphere ($\mathbf{R}=0$) $f_{\nu L0}$ is nonzero only if Y_L contains a part which transforms like a_ν itself (1.9). If we choose $l_{\max}=2$, this is true for one L only.

While the second part varies smoothly with $\mathbf{r}$, the first part describes the oscillations of the Wannier functions at the lattice sites where the potential is singular. The radial functions $f_{\nu L\mathbf{R}}$ can be represented by cubic spline functions. In cases where it seems to be appropriate the plane wave part as well may be expanded into spherical harmonics around any point in $\mathbf{r}$ space particularly around any lattice site.

III. RESULTS

We considered the fcc transition metals Ni (paramagnetic), Cu, Pd, Ag, Pt, and Au. The Bloch functions were obtained from MAPW calculations in the local density approximation using the density functional according to Gunnarsson and Lundquist.[13] The shape of the effective potential was assumed to be warped muffin tin. For the $4d$ and $5d$ metals a scalar-relativistic version[14] based on the Foldy-Wouthuysen[15] transformation was applied with the relativistic correction to the exchange potential according to Macdonald and Vosko.[16]

For the various metals we considered a nine dimensional band complex defined by the representations Γ_1, Γ_{12}, $\Gamma_{25'}$, and Γ_{15} at the point $\mathbf{k}=0$. The artificial cut leads of course to inaccuracies in the reproduction of the band structure at the upper edge of the band complex but it can be expected that this will affect only the p-like Wannier functions belonging to the high-lying Γ_{15} representation.

A. Coefficients of the model Hamiltonian

In the first step the Slater-Koster-parameters of the model Hamiltonian had to be determined. We performed a fit to the band structure energies including 110 equidistant $\mathbf{k}$ points in the irreducible wedge of the Brillouin zone. During the iteration process the mean error was calculated considering only eigenvalues up to a certain limiting energy. This energy limit was raised as long as the error below the preceding limit was not significantly increased. The effect of this procedure is that the fit is excellent below the energy limit and slowly becomes worse with increasing energy. We want to stress that this method is to be preferred to the method of Papaconstantopoulos,[17] who took the energy Γ_{15} at the

TABLE I. Mean error for the Slater-Koster interpolation in the region below the given energy limits in mRy.

Energy limit	Ni	Cu	Pd	Ag	Pt	Au
Fermi energy	0.24	0.33	0.22	0.34	0.24	0.33
Fermi energy + 0.4 Ry	0.29	0.41	0.33	0.40	0.27	0.42
Fermi energy + 0.7 Ry	0.88	2.38	4.27	2.24	0.98	3.81

TABLE II. Slater-Koster parameters.

	Ni	Cu	Pd	Ag	Pt	Au
$E_{s,s}(000)$	0.79550	0.96850	1.13270	1.27040	1.01250	0.90700
$E_{3z^2-r^2,3z^2-r^2}(000)$	0.33740	0.50840	0.55240	0.77760	0.59750	0.54210
$E_{yz,yz}(000)$	0.34180	0.51820	0.55670	0.78570	0.60070	0.57310
$E_{x,x}(000)$	1.30560	1.47900	1.53970	1.68280	1.59770	1.52900
$E_{s,s}(110)$	-0.08070	-0.08960	-0.08000	-0.06220	-0.07210	-0.06650
$E_{3z^2-r^2,s}(110)$	0.00620	0.00840	-0.01930	-0.01480	-0.04190	-0.01090
$E_{3z^2-r^2,3z^2-r^2}(110)$	-0.00910	-0.01190	-0.01660	-0.01020	-0.01650	-0.01530
$E_{x^2-y^2,x^2-y^2}(110)$	0.01870	0.02460	0.02800	0.01760	0.02390	0.02810
$E_{yz,yz}(110)$	0.00710	0.00810	0.00960	0.00630	0.01030	0.00980
$E_{zy,yz}(110)$	0.00910	0.01090	0.01270	0.00790	0.01210	0.00610
$E_{xy,s}(110)$	-0.03410	-0.04160	0.04800	0.03310	0.05150	0.05240
$E_{xy,3z^2-r^2}(110)$	0.01040	0.01440	0.02420	0.01320	0.02310	0.02190
$E_{xy,xy}(110)$	-0.02060	-0.02700	-0.04060	-0.02450	-0.04190	-0.03890
$E_{x,s}(110)$	-0.08610	-0.08790	0.08370	0.06640	0.08570	0.07670
$E_{x,3z^2-r^2}(110)$	0.00520	0.00800	0.02810	0.01390	0.04030	0.01280
$E_{x,x^2-y^2}(110)$	0.01950	0.02270	0.01940	0.01370	0.01280	0.02780
$E_{x,xy}(110)$	-0.02910	-0.03610	-0.04530	-0.03330	-0.05340	-0.05810
$E_{x,x}(110)$	0.08340	0.08340	0.06340	0.05660	0.06850	0.08210
$E_{y,x}(110)$	0.10280	0.10060	0.10670	0.07700	0.10960	0.10200
$E_{z,yz}(110)$	0.00650	0.01200	0.01520	0.00930	0.01130	0.00580
$E_{z,z}(110)$	0.02370	0.01690	-0.01490	-0.00200	-0.00910	0.00230
$E_{s,s}(002)$	0.00860	0.00310	0.00280	0.00330	0.00230	0.01210
$E_{3z^2-r^2,s}(002)$	-0.00580	-0.00820	0.00710	0.00000	-0.00200	-0.00160
$E_{3z^2-r^2,3z^2-r^2}(002)$	-0.00520	-0.00650	-0.00350	-0.00310	-0.00280	-0.00390
$E_{x^2-y^2,x^2-y^2}(002)$	-0.00130	-0.00180	-0.00550	-0.00080	0.00180	-0.00300
$E_{yz,yz}(002)$	0.00140	0.00090	0.00130	0.00010	-0.00040	-0.00340
$E_{xy,xy}(002)$	0.00010	0.00030	0.00090	0.00040	0.00100	0.00090
$E_{x,zy}(002)$	-0.00010	-0.00100	0.00230	-0.00060	-0.00010	-0.00390
$E_{x,x}(002)$	0.01160	0.00950	-0.01710	0.00030	-0.00070	0.00690
$E_{z,s}(002)$	0.00680	0.00170	-0.00680	-0.00040	-0.00760	-0.01120
$E_{z,3z^2-r^2}(002)$	-0.00750	-0.01030	-0.01150	-0.00200	0.00130	-0.00280
$E_{z,z}(002)$	-0.00190	0.00260	-0.00710	0.00970	-0.01310	0.00040
$E_{s,s}(112)$	0.00000	0.00340	-0.00100	-0.00060	-0.00180	-0.00310
$E_{3z^2-r^2,s}(112)$	-0.00040	-0.00050	0.00150	0.00070	0.00030	0.00080
$E_{3z^2-r^2,3z^2-r^2}(112)$	-0.00040	-0.00050	-0.00060	-0.00010	0.00050	-0.00100
$E_{x^2-y^2,x^2-y^2}(112)$	0.00040	0.00050	0.00150	0.00020	-0.00030	0.00090
$E_{yz,s}(112)$	-0.00040	0.00050	-0.00070	0.00030	0.00030	0.00090
$E_{yz,3z^2-r^2}(112)$	-0.00020	0.00000	0.00070	0.00000	0.00040	0.00050
$E_{yz,x^2-y^2}(112)$	-0.00030	-0.00050	-0.00070	-0.00020	0.00010	-0.00090
$E_{yz,yz}(112)$	-0.00030	0.00020	0.00050	0.00010	0.00020	0.00000
$E_{zy,x^2-y^2}(112)$	0.00030	0.00050	0.00070	0.00020	-0.00010	0.00090
$E_{zy,yz}(112)$	-0.00010	-0.00010	0.00010	-0.00020	-0.00060	0.00040
$E_{xy,s}(112)$	-0.00070	0.00000	-0.00100	-0.00030	0.00020	-0.00050
$E_{xy,3z^2-r^2}(112)$	-0.00010	0.00020	0.00110	0.00010	0.00040	0.00050
$E_{xy,yz}(112)$	-0.00020	0.00010	0.00030	0.00010	0.00020	0.00010
$E_{xy,xy}(112)$	0.00000	0.00010	0.00030	0.00010	0.00020	0.00020
$E_{x,s}(112)$	-0.00250	0.00080	-0.00120	0.00080	0.00150	0.00200
$E_{x,3z^2-r^2}(112)$	0.00070	0.00120	0.00150	-0.00020	-0.00040	0.00130
$E_{x,x^2-y^2}(112)$	0.00060	0.00080	0.00110	0.00010	-0.00020	0.00120
$E_{x,yz}(112)$	0.00020	0.00060	-0.00050	-0.00030	-0.00100	-0.00070
$E_{x,zy}(112)$	-0.00060	0.00000	0.00060	0.00010	0.00030	-0.00020
$E_{x,xy}(112)$	-0.00070	0.00020	0.00080	0.00000	-0.00020	-0.00040
$E_{x,x}(112)$	0.00100	0.00060	-0.00340	-0.00090	-0.00130	0.00080
$E_{y,x}(112)$	0.00500	0.00140	0.00000	0.00100	0.00190	0.00450
$E_{z,s}(112)$	0.00240	0.00450	0.00080	-0.00140	-0.00040	0.00340
$E_{z,3z^2-r^2}(112)$	-0.00010	0.00010	-0.00160	-0.00050	-0.00040	0.00030
$E_{z,yz}(112)$	-0.00040	0.00140	0.00150	0.00000	0.00030	-0.00050
$E_{z,xy}(112)$	-0.00020	0.00100	0.00060	0.00080	-0.00050	0.00120
$E_{z,x}(112)$	0.00170	-0.00180	-0.00070	0.00010	0.00050	0.00220
$E_{z,z}(112)$	-0.01180	-0.01120	0.00000	-0.00650	-0.00700	0.00110

upper edge of the band complex and other p-like states at symmetry points into account in every step of iteration. It is not possible to reproduce these high-lying states in this nine dimensional model without affecting the lower part of the band structure because this Γ_{15} level is hybridized with another Γ_{15} level following 0.8 Ry above, so there should be even on-site matrix elements between these two in an extended model. Three shells of neighbors have been taken into account. The mean error is given in Table I. The values given could be verified for arbitrary $\mathbf{k}$ meshes. In general it can be said that the fit is excellent in the region up to 0.5 Ry above the Fermi level. It shall be mentioned that a mean error of only 3 mRy could be obtained with only nearest neighbors taken into account. The values for the Slater-Koster parameters are given in Table II. The first-principles band structure and the interpolated one are compared in Fig. 1.

The conclusion to be drawn from these results is that it is well possible to achieve good convergence of the Slater-Koster parameters in an orthogonal basis and that it is not necessary to introduce a nonorthogonal basis to reproduce a first-principles band structure with high accuracy.

The procedure can be generalized for the case when spin orbit coupling is included leading to Wannier functions transforming under representations of double groups. This will be the subject of a future paper.

B. Localization

An appropriate measure for the localization of the Wannier functions is the mean value of r^2 already used for the determination of the phases of the Bloch functions. If we define

$$I_{\nu\mu}(\mathbf{k},\mathbf{q}) \equiv \int_{\mathrm{WSC}} \phi^*_{\nu\mathbf{k}}(\mathbf{r})\, e^{-i\mathbf{q}\cdot\mathbf{r}}\, \phi_{\mu\mathbf{k}+\mathbf{q}}(\mathbf{r})\, d\mathbf{r} \tag{3.1}$$

(where WSC denotes the Wigner-Seitz cell), then we can write instead of (2.11):

$$r^2_{\nu\nu} = -\left(\Delta_{\mathbf{q}}\, \frac{1}{d} \sum_{\mu\in\Gamma^{(p)}} \frac{\Omega}{(2\pi)^3} \int_{\mathcal{BZ}} I_{\mu\mu}(\mathbf{k},\mathbf{q})\, d\mathbf{k}\right)_{\mathbf{q}=0} \quad \text{for } \nu \in \Gamma^{(p)} \quad , \tag{3.2}$$

employing the Laplace operator with respect to $\mathbf{q}$ at the point $\mathbf{q} = 0$. The sum over all rows of $\Gamma^{(p)}$ leads to cubic symmetry in $\mathbf{q}$, which permits a quadratic approximation for small q:

$$r^2_{\nu\nu} = \frac{3}{q^2}\, \frac{1}{d} \sum_{\mu\in\Gamma^{(p)}} \frac{\Omega}{(2\pi)^3} \int_{\mathcal{BZ}} [\, I_{\mu\mu}(\mathbf{k},\mathbf{q}) - 1\,]\, d\mathbf{k} \quad . \tag{3.3}$$

Results for the root of the mean square radius obtained with q of order 10^{-3} are given in Table III.

Another measure is the probability integral restricted to the muffin-tin sphere (MTS),[6] where the Wannier function is centered:

$$P_\nu = \int_{\mathrm{MTS}} |\, a_\nu(\mathbf{r})\,|^2 d^3r \quad . \tag{3.4}$$

Values for P_ν are given in Table IV . The $\mathbf{k}$-space integrations were performed with 110 points in the irreducible wedge to obtain the results in Tables III and IV. The effect of the number of $\mathbf{k}$ points on the shape of the Wannier functions in the central cell is very small while it becomes larger for increasing values of $\mathbf{r}$. If $\mathbf{k}$ points with degeneracies are contained in the integration mesh the procedure of Sec. II A has to be applied to give the correct results.

These results show that the d-like Wannier functions are almost completely localized in the central Wigner-Seitz cell for all the metals considered. It is observed that the localization of the s function is strongly increased with the strength of relativistic effects, while the d functions become slightly more delocalized. This is in agreement with the general observation that the binding of s states is stressed by relativistic effects leading at the same time to an increased screening of the potential for d-like states.

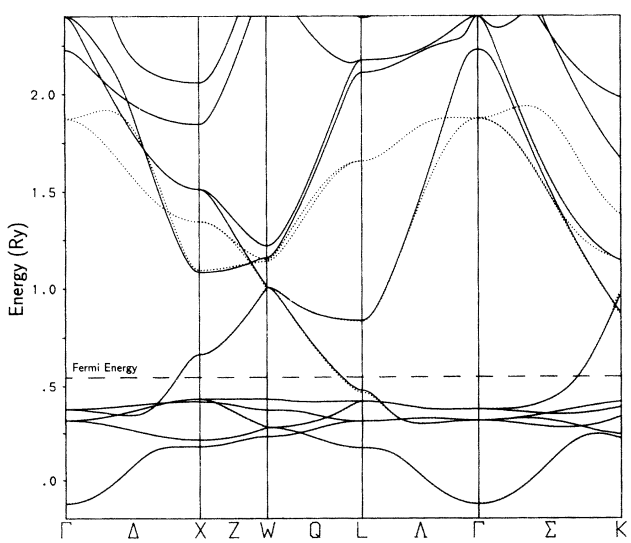

FIG. 1. Band structure of copper in directions of high symmetry in the Brillouin zone. The solid curves show the first-principles energies and the dotted curves the eigenvalues of the model Hamiltonian. The fit is excellent in the region up to 0.5 Ry above the Fermi level. The level Γ_{15} at 2.4 Ry cannot be reproduced in this model.

TABLE III. Square root of the mean square radius of the Wannier functions $\langle r^2\rangle^{\frac{1}{2}}$ in a.u.

	Γ_1	Γ_{12}	$\Gamma_{25'}$	Γ_{15}	Lattice constant	MT radius
Ni	5.5	1.1	1.1	10.3	6.652	2.352
Cu	6.7	1.2	1.3	10.0	6.831	2.415
Pd	5.2	1.3	1.3	8.6	7.328	2.591
Ag	5.6	1.2	1.2	11.1	7.789	2.754
Pt	4.3	1.4	1.3	8.9	7.399	2.616
Au	3.7	1.6	1.8	10.9	7.679	2.715

TABLE IV. Probability integral P_ν restricted to the central muffin-tin sphere.

	Γ_1	Γ_{12}	$\Gamma_{25'}$	Γ_{15}
Ni	0.42	0.95	0.97	0.23
Cu	0.39	0.96	0.97	0.23
Pd	0.56	0.94	0.95	0.23
Ag	0.64	0.96	0.97	0.31
Pt	0.68	0.95	0.95	0.28
Au	0.70	0.94	0.96	0.32

The lack of systematics in the values for the p functions is probably due to inaccuracies caused by the cut at the upper edge of the band complex defined by the model Hamiltonian. This would have to be accounted for by an extension of the model Hamiltonian.

The behavior of the Wannier functions is illustrated by the plots in the next-neighbor direction (011), which is the direction of slowest falloff, in Figs. 2–4. The curves have been obtained using 1012 **k** points in the irreducible wedge. It can be seen that the number of nodes between the origin and the neighboring lattice site is increased by one going from the $3d$ to the $4d$ metals and from the $4d$ to the $5d$ metals, respectively. The Wannier functions show distinctive oscillations at the noncentral lattice sites, which are expected from the orthogonality relations (1.10). Figure 2 shows that in the case of the s function the amplitudes of these oscillations fall off much faster for the heavier metals, in agreement with the results from Tables III and IV. Figure 3 exhibits the opposite tendency for the d functions, although on a much lower scale.

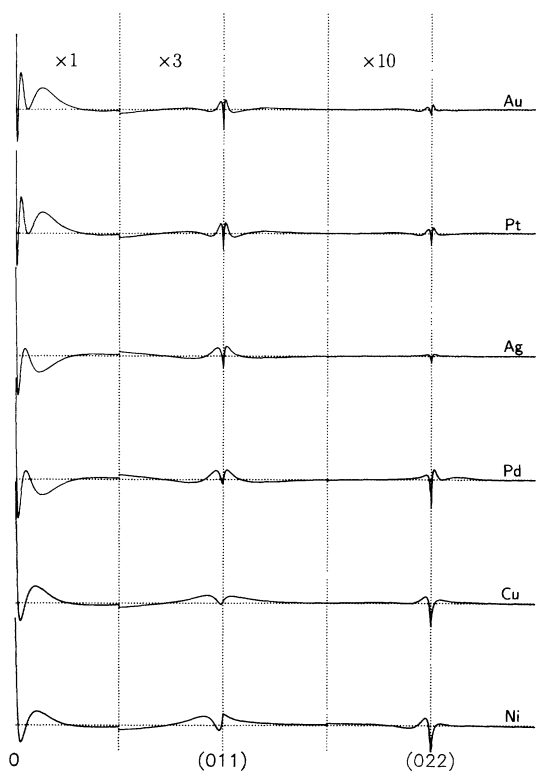

FIG. 2. Wannier function of s symmetry (Γ_1) plotted in the (011) direction. For clarity the plot starts a small distance away from the origin. The function value has been multiplied by a factor 3 in the muffin-tin sphere around the lattice point $(011)a/2$ and by a factor 10 in the sphere around $(022)a/2$. (a denotes the lattice constant.) The falloff is increased with the strength of relativistic effects.

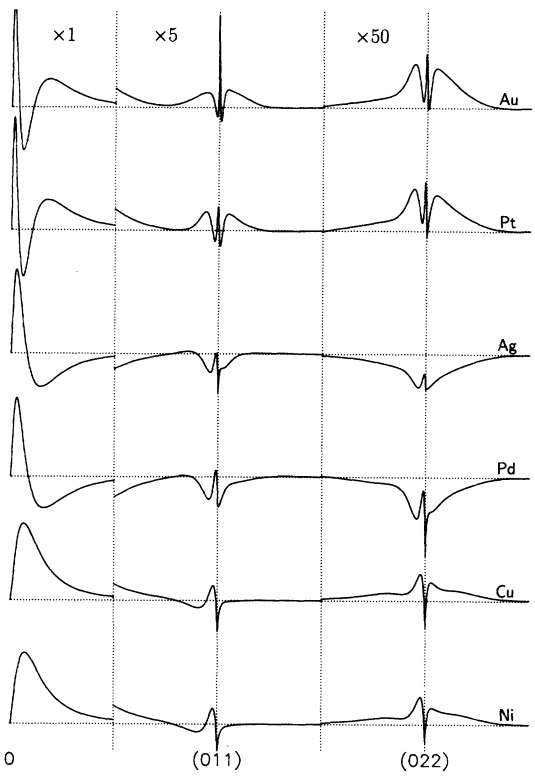

FIG. 3. Wannier function of yz symmetry ($\Gamma_{25'}$) plotted in the (011) direction. The function value has been multiplied by a factor 5 in the muffin-tin sphere around the lattice point $(011)a/2$ and by a factor 50 in the sphere around $(022)a/2$.

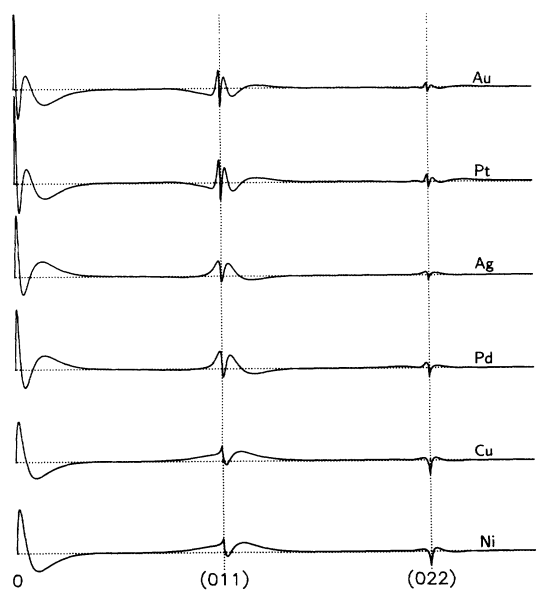

FIG. 4. Wannier function of z symmetry (Γ_{15}) plotted in the (011) direction.

TABLE V. Overlap $S_n^{(p)}$ between bands and representations for Cu.

Band	Γ_1	Γ_{12}	$\Gamma_{25'}$	Γ_{15}
1	0.260	0.354	0.302	0.083
2	0.009	0.277	0.684	0.027
3	0.026	0.238	0.686	0.047
4	0.012	0.589	0.379	0.019
5	0.009	0.310	0.677	0.002
6	0.167	0.216	0.227	0.385
7	0.301	0.003	0.039	0.662
8	0.183	0.005	0.003	0.809
9	0.030	0.006	0.001	0.964

C. Energy spreading

The results obtained above show that the concept of the band complex, which implies appropriate linear combinations of Bloch states belonging to different bands, yields Wannier functions having not only good symmetry but also the desired localization properties. It might be of interest to consider the relationship with the bands in the ordinary sense. As a measure for the overlap between a band n and a representation $\Gamma^{(p)}$ we can define the following integral:

$$S_n^{(p)} = \sum_{\nu\in\Gamma^{(p)}} \int_{BZ} |e(n,\mathbf{k})_\nu|^2 \, d\mathbf{k}. \tag{3.5}$$

Values for these integrals are given in Table V for the case of copper. Clearly the d-like representations Γ^{12} and $\Gamma^{25'}$ play a dominant role in the first six bands and almost disappear in the upper three ones, which show mainly Γ^{15} symmetry. Γ^1 appears to a considerable amount in bands 1, 6, 7, and 8. The strong mixing of symmetries especially in bands 1 and 6 shows the necessity for the inclusion of all three symmetry types in the band complex.

SUMMARY

We have shown how Wannier functions can be constructed from first-principles Bloch functions with high accuracy. They are orthogonal to each other as well as to the core states and are everywhere differentiable. The precondition for this transformation was the accurate determination of the parameters of the Slater-Koster interpolation scheme in the orthogonal basis. At points of degeneracies the resulting eigenvectors had to be adapted to the Bloch functions. The combination of the two yielded smooth functions in $\mathbf{k}$ space and thus localized Wannier functions.

The results for fcc transition metals show highly localized functions of d symmetry, an s function whose localization is strongly increased with the strength of relativistic effects, and less localized p functions.

The Wannier functions can be calculated with reasonable computational effort in the central and the neighboring cells and may now be used in various applications.

ACKNOWLEDGMENTS

Thanks are due to Dr. H. Reinisch for his relativistic band structure calculations.

APPENDIX

Let β be a member of $G(\mathbf{k})$. From (2.1) we have

$$\begin{aligned} a_\nu(\beta^{-1}\mathbf{r}) &= \int d\mathbf{k} \sum_n e(n,\mathbf{k})_\nu \psi_{n\mathbf{k}}(\beta^{-1}\mathbf{r}) \\ &= \sum_n e(n,\mathbf{k})_\nu \sum_{n'} \widetilde{D}_{\mathbf{k}}(\beta)_{nn'} \psi_{n'\mathbf{k}}(\beta^{-1}\mathbf{r}). \end{aligned} \tag{A1}$$

Because of (1.9) this has to be equal to

$$\begin{aligned} &\sum_\mu \Gamma(\beta^{-1})_{\nu\mu} a_\mu(\mathbf{r}) \\ &\qquad = \sum_\mu \Gamma(\beta^{-1})_{\nu\mu} \int d\mathbf{k} \sum_n e(n,\mathbf{k})_\nu \psi_{n\mathbf{k}}(\mathbf{r}). \end{aligned} \tag{A2}$$

From (2.2) it follows that

$$\sum_n \widetilde{D}_{\mathbf{k}}(\beta)_{nn'} e(n,\mathbf{k})_\nu = \sum_\mu \Gamma(\beta^{-1})_{\nu\mu} e(n',\mathbf{k})_\mu. \tag{A3}$$

The unitarity of the eigenvectors $e(n,\mathbf{k})$ gives

$$\widetilde{D}_{\mathbf{k}}(\beta)_{nn'} = \sum_\mu \Gamma(\beta^{-1})_{\nu\mu} e(n',\mathbf{k})_\mu e(n,\mathbf{k})_\nu. \tag{A4}$$

Together with (2.3) this yields (2.5).

[1] G. Wannier, Phys. Rev. **52**, 191 (1937).
[2] W. Kohn, Phys. Rev. B **7**, 4388 (1973).
[3] P. Modrak and R. Wojnecki, Phys. Rev. B **36**, 5830 (1987); Phys. Status Solidi B **152**, 203 (1989).
[4] P. Modrak, Phys. Rev. B **46**, 15 716 (1992).
[5] J. Callaway and A.J. Hughes, Phys. Rev. **156**, 860 (1967); **164**, 1043 (1967).
[6] D.A. Goodings and R. Harris, Phys. Rev. **178**, 1189 (1969).
[7] E.I. Blount, Solid State Phys. **13**, 305 (1962).
[8] J. Des Cloizeaux, Phys. Rev. **135**, A685 (1964).
[9] H. Bross, Z. Phys. **243**, 311 (1971).
[10] H. Teichler, Phys. Status Solidi B **43**, 307 (1971).
[11] H. Bross, G. Bohn, G. Meister, W. Schubö, and H. Stöhr, Phys. Rev. B **2**, 3098 (1970).
[12] H. Bross and R. Eder, Phys. Status Solidi B **144**, 175 (1987).
[13] O. Gunnarsson and B.I. Lundquist, Phys. Rev. B **13**, 4274 (1976).
[14] H. Reinisch and H. Bross, J. Phys. Condensed Matter **5**, 977 (1993).
[15] L.L. Foldy and S.A. Wouthuysen, Phys. Rev. **78**, 29 (1950).
[16] A.H. Macdonald and S.H. Vosko, J. Phys. C **12**, 2977 (1979).
[17] D.A. Papaconstantopoulos, *Handbook of the Band Structure of Elemental Solids* (Plenum, New York, 1986).